

Asymptotic solutions for optical properties of large particles with strong absorption

Ping Yang, Bo-Cai Gao, Bryan A. Baum, Yong X. Hu, Warren J. Wiscombe, Michael I. Mishchenko, Dave M. Winker, and Shaima L. Nasiri

The transverse wave condition is not applicable to the refracted electromagnetic wave within the context of geometrical optics when absorption is involved. Either the TM or the TE wave condition can be assumed for the wave to locally satisfy the electromagnetic boundary condition in a ray-tracing calculation. The assumed wave mode affects both the reflection and the refraction coefficients. As a result, nonunique solutions for these coefficients are inevitable. In this study the appropriate solutions for the Fresnel reflection–refraction coefficients are identified in light-scattering calculations based on the ray-tracing technique. In particular, a 3×2 refraction or transmission matrix is derived to account for the inhomogeneity of the refracted wave in an absorbing medium. An asymptotic solution that completely includes the effect of medium absorption on Fresnel coefficients is obtained for the scattering properties of a general polyhedral particle. Numerical results are presented for hexagonal plates and columns with both preferred and random orientations. © 2001 Optical Society of America

OCIS codes: 010.1290, 010.1310, 010.3920, 290.5850, 290.1090, 280.1310.

1. Introduction

The optical properties of dielectric particles such as aerosols and ice crystals in the atmosphere are fundamental to a number of disciplines, including atmospheric radiation transfer and airborne or satelliteborne remote-sensing applications. In a recent book¹ Mishchenko *et al.* comprehensively reviewed various methods that have been developed to solve the scattering and absorption properties of particles for a variety of geometric morphologies and

electromagnetic characteristics of the scatterers. Accurate numerical methods such as the discrete dipole approximation method^{2,3} and the finite-difference time-domain (FDTD) technique^{4,5} are applicable in practice only to size parameters smaller than 20 because the computational requirements increase quickly with size parameter. Although analytical solutions are available for some particle shapes, such as spheres⁶ and spheroids,^{7,8} the corresponding numerical computations are usually quite challenging. For example, the computation of the optical properties of spheroids based on an analytical solution in terms of a series of special functions may not be stable when the size parameter is larger than approximately 30–40. It is worth noting that recent developments for the T-matrix method^{9,10} permit exact solutions for the optical properties of spheroids and finite circular cylinders for size parameters up to 200.¹¹ There is no single method to solve for the optical properties of nonspherical particles across the entire size parameter spectrum.

It is common to use the ray-tracing technique^{12–15} for nonspherical particles that have sizes much larger than the incident wavelength. Previous applications of the ray-tracing technique were focused primarily on scattering computations for the visible and near-infrared wavelengths, for which the imaginary part of the refractive index is small. For these weakly absorptive spectra, the conventional Snell

P. Yang (pyang@climate.gsfc.nasa.gov) and W. J. Wiscombe are with the NASA Goddard Space Flight Center, Code 913, Greenbelt, Maryland 20771. P. Yang is also with Science Systems and Applications, Inc., Suite 300, 5900 Princess Garden Parkway, Lanham, Maryland 20706. B.-C. Gao is with the Remote Sensing Division, Code 7212, U.S. Naval Research Laboratory, Washington, D.C. 20375. B. A. Baum, Y. X. Hu, and D. M. Winker are with the Atmospheric Sciences Division, MS 420, NASA Langley Research Center, Hampton, Virginia 23681. M. I. Mishchenko is with the NASA Goddard Institute for Space Studies, 2880 Broadway, New York, New York 10025. S. L. Nasiri is with the Cooperative Institute for Meteorological Satellite Studies, University of Wisconsin–Madison, 1225 West Dayton Street, Madison, Wisconsin 53706.

Received 11 July 2000; revised manuscript received 29 November 2000.

0003-6935/01/091532-16\$15.00/0

© 2001 Optical Society of America

law and Fresnel formulas can be used to account for ray reflection and refraction at the particle surface. However, the optical properties of large dielectric particles at wavelengths with strong absorption are fundamental to many practical applications. For example, the scattering and absorption properties of ice crystals at infrared wavelengths must be known for the retrieval of cirrus clouds by use of satellite radiance data such as that from the Advanced Very High Resolution Radiometer¹⁶ (AVHRR) and the Moderate Resolution Imaging Spectroradiometer¹⁷ (MODIS) imagers. Under conditions of cirrus clouds, interpretation of information from the High Resolution Interferometer Sounder¹⁸ (HIS) hyperspectrum in the atmospheric window region (8–12 μm) also requires knowledge of the optical properties of ice crystals.

When ray optics is applied to the infrared spectrum in regions of strong absorption, the refracted wave inside the particle is inhomogeneous in the sense that the planes of constant phase and constant amplitude are not parallel.¹⁹ Current applications of the ray-tracing technique assume that planes of constant phase and constant amplitude are parallel. The inhomogeneity associated with the reflected wave substantially complicates the behavior of rays at the particle surface and inside the medium. Stratton¹⁹ and Born and Wolf²⁰ have discussed this inhomogeneity and its effect on the Fresnel reflection coefficients associated with a complex refractive index. In particular, Stratton¹⁹ (Ref. 19, Section 9.9) has solved the problem of the reflection of a plane electromagnetic wave by a conducting surface. Recently, Zhang and Xu²¹ and Yang and Liou²² addressed the effect of an inhomogeneous wave on the ray-tracing calculation. Zhang and Xu²¹ expressed the Fresnel coefficients without explicit use of the complex refractive index. However, they did not account for the effect of the inhomogeneity on wave attenuation that is the most important physical process involved in ray propagation within an absorbing medium. Yang and Liou²² discussed the result of the inhomogeneous effect on ray propagation by introducing an effective refractive index, but they employed the high-frequency approximation²⁰ in the calculation of reflection and refraction coefficients. Inasmuch as the effect of inhomogeneity on the ray-tracing calculation has not been solved completely, it is necessary to study this problem further. Our intent in this study is to develop an analytical asymptotic method that comprehensively accounts for the inhomogeneity effect when the optical properties (such as the single-scattering albedo and the phase function) of strongly absorbing particles with sizes much greater than the incident wavelength are derived.

To compute the optical properties of dielectric particles with strong absorption we first derive the reflection and refraction coefficients for the electric field in terms of an apparent refractive index without using the high-frequency approximation. The reflection and refraction coefficients incorporate the

inhomogeneous effect on the direction of ray propagation and the Fresnel coefficients. Subsequently, we derive the asymptotic solution expressed in an analytical form for large particles with strong absorption. In Section 2 we discuss the various wave modes of an inhomogeneous wave refracted into a particle when absorption is involved. We show that the electric or magnetic field may not be perpendicular to the direction of ray propagation because of the effect of strong absorption. The Fresnel coefficients, in particular the transmission coefficient for the component of the refracted field that is parallel to ray propagation, are reformulated. In Section 3 we present the analytical solution for the optical properties of large polyhedral particles with strong absorption. The solution is derived on the basis of the electromagnetic relationship between the near field and the far field. In Section 3 we also present numerical results of the asymptotic solution for hexagonal ice crystals. Finally, conclusions of this study are given in Section 4.

2. Physical Basis for Ray Tracing in the Absorptive Case

In this section it is shown that the transverse wave condition cannot be applied to both the electric and the magnetic fields associated with a ray refracted into an absorbing medium. In addition, we show that a wave mode subject to an electric boundary condition is not unique within the context of geometrical optics when absorption is involved. The behavior of the refracted wave affects not only the Fresnel refraction coefficients but also the Fresnel reflection coefficients. In the following discussion it is shown that there are four possible combinations of reflection–refraction coefficients that depend on wave modes. Whereas each combination of reflection and refraction coefficients is a mathematically rational solution, only one set of coefficients should be used in the ray-tracing solution. The choice of the proper wave mode for the refracted wave in a ray-tracing calculation is made through comparison of the geometrical-optics solution and the analytical Mie result for the scattering properties of a very large (size parameter of the order of 1000) sphere with strong absorption.

Let us consider the application of the geometrical-optics method to solve for the scattering properties of a particle that is large and absorptive. In this case, the rays that are refracted into the particle are largely absorbed. Thus we need consider only the first-order reflected–refracted rays because of the small amount of energy carried by the rays that undergo internal reflections. To examine the first-order reflection–refraction characteristics and the corresponding polarization features of the electric field, we begin with the phase variation for the field associated with a complex refractive index. Let three unit vectors, \hat{e}_i , \hat{e}_r , and \hat{e}_t , indicate the propagating directions for the incident, reflected, and refracted rays, respectively. To present this study systematically, we must recapitulate some results ob-

tained by Yang and Liou.²² Following those authors, the fields associated with these rays can be written as follows:

$$\mathbf{E}_i(\mathbf{r}) = \mathbf{E}_{i_0} \exp(ik\hat{e}_i \cdot \mathbf{r}), \quad (1a)$$

$$\mathbf{E}_r(\mathbf{r}) = \mathbf{E}_{r_0} \exp(ik\hat{e}_r \cdot \mathbf{r}), \quad (1b)$$

$$\mathbf{E}_t(\mathbf{r}) = \mathbf{E}_{t_0} \exp[ik(N_r\hat{e}_t + iN_n\hat{n}) \cdot \mathbf{r}], \quad (1c)$$

where \mathbf{E}_{i_0} , \mathbf{E}_{r_0} , and \mathbf{E}_{t_0} are the amplitude vectors for the fields; $k = 2\pi/\lambda$, in which λ is the wavelength in vacuum; and \hat{n} is a unit vector that is normal to the particle surface and to points into the particle. The parameters N_r and N_n in Eq. (1c) are given by

$$N_r = 2^{-1/2}\{m_r^2 - m_i^2 + \sin^2 \zeta_i + [(m_r^2 - m_i^2 - \sin^2 \zeta_i)^2 + 4m_r^2 m_i^2]^{1/2}\}^{1/2}, \quad (1d)$$

$$N_n = 2^{-1/2}\{-(m_r^2 - m_i^2 - \sin^2 \zeta_i) + [(m_r^2 - m_i^2 - \sin^2 \zeta_i)^2 + 4m_r^2 m_i^2]^{1/2}\}^{1/2}, \quad (1e)$$

in which m_r and m_i are the real and the imaginary parts, respectively, of the refractive index and ζ_i is the incident angle, given by $\zeta_i = \sin^{-1}[1 - (\hat{e}_i \cdot \hat{n})^2]^{1/2}$. Note that N_n (denoted N_i^* in Ref. 22) was not presented in the previous study. Physically, N_r is the parameter that determines the phase and N_n is the parameter that determines the absorption, as we illustrate in the following discussion.

From Eqs. (1a)–(1c) and the continuity of the wave phase at the medium interface, it follows that Snell's law for an absorbing medium can be mathematically expressed in the form

$$\hat{e}_r = \hat{e}_i + 2(\hat{e}_i \cdot \hat{n})\hat{n}, \quad (2a)$$

$$\hat{e}_t = \hat{e}_i/N_r + (\cos \zeta_t - \cos \zeta_i/N_r)\hat{n}, \quad (2b)$$

where the refractive angle is given by $\zeta_t = \sin^{-1}[\sin(\zeta_i)/N_r]$. Equation (2a) means that the incident and reflected rays are spatially symmetric about the direction normal to the particle surface at the incident point, which is the standard Snell law for the reflection direction. However, Eq. (2b) indicates that the refracted direction is determined not by m_r but by N_r . For this reason, N_r is referred to as the real part of the apparent refractive index, which depends on the incident configuration and the dielectric constant of the medium for determining the direction and the phase of a refracted wave. The attenuation of a refracted field as a result of absorption depends on the direction of observation. If the direction is along \hat{n} , the attenuation is determined by N_n , as is evident from Eq. (1c). However, if we trace the refracted wave along the direction of the refracted ray, i.e., along position vector $\mathbf{r} = l\hat{e}_t$, in which l is the penetration depth of the ray, the electric field is given by

$$\mathbf{E}_i(l\hat{e}_t) = \mathbf{E}_{t_0} \exp[-kN_n(\hat{n} \cdot \hat{e}_t)l] \exp(ikN_r l). \quad (3)$$

Obviously, the factor $N_n(\hat{n} \cdot \hat{e}_t)$ is the imaginary part of the apparent refractive index that governs the at-

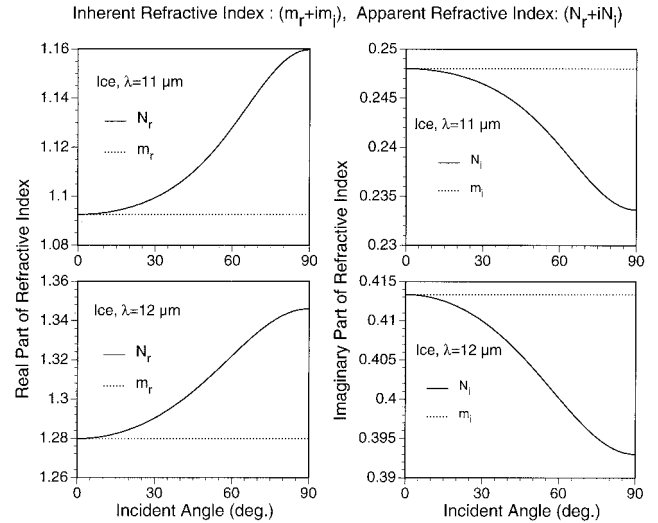


Fig. 1. Comparison of the inherent and apparent refractive indices for ice at 11 and 12 μm .

tenuation of the electric field associated with the rays. We denote this factor N_i . Thus, for a ray that impinges upon an absorbing medium, the apparent refractive index in the complex format is $(N_r + iN_i)$. It can be proved that

$$N_i = N_n(\hat{n} \cdot \hat{e}_t) = N_n \cos \zeta_t = m_r m_i / N_r. \quad (4)$$

Figure 1 shows the real and imaginary parts of the inherent and apparent refractive indices of ice at infrared wavelengths of 11 and 12 μm , for which substantial absorption exists. The optical properties of ice at these two wavelengths are important for many applications in satellite remote sensing.¹⁷ Note that, for ice particles, wavelengths near 11 μm are in the Christiansen band, where absorption dominates the extinction.²³ The inherent refractive index is determined uniquely by the dielectric characteristic of the medium, i.e., permittivity, which does not depend on the incident configuration of a ray. As is shown in Fig. 1, the real part of the apparent refractive index increases with the increase of incident angle, whereas the imaginary part of the refractive index decreases with the increase of the incident angle. Obviously, in terms of wave attenuation per unit length along the propagation direction of a ray, the particle is less absorptive at a large incident angle. For incident angles larger than 10°, the inhomogeneous effect that is due to strong absorption on both real and imaginary parts of the refractive index becomes noticeable.

We can show that various wave modes could satisfy the electromagnetic boundary condition associated with reflection and refraction at the interface of two media, one of which is strongly absorptive. First, let $\hat{\beta}$ be a unit vector perpendicular to the incident plane. The unit vectors that are parallel to the incident plane and perpendicular to ray propagation direc-

tions for the incident, reflected, and refracted waves are given by

$$\hat{\alpha}_i = \hat{e}_i \times \hat{\beta}, \quad \hat{\alpha}_r = \hat{e}_r \times \hat{\beta}, \quad \hat{\alpha}_t = \hat{e}_t \times \hat{\beta}. \quad (5)$$

It should be pointed out that $\hat{\beta}\hat{\alpha}_{i,r,t}\hat{e}_{i,r,t}$ constitute right-handed coordinate systems. The incident and reflected waves are within the nonabsorbing medium. As a result of the homogeneous wave properties of the incident and reflected rays, the condition of a transverse wave (hereafter referred to as the TEM mode) can be imposed on both electric and magnetic fields for these rays. Thus the corresponding amplitude vectors of the electric fields can be decomposed in the form

$$\mathbf{E}_{io} = E_{io,\alpha}\hat{\alpha}_i + E_{io,\beta}\hat{\beta}, \quad (6a)$$

$$\mathbf{E}_{ro} = E_{ro,\alpha}\hat{\alpha}_r + E_{ro,\beta}\hat{\beta}. \quad (6b)$$

The Maxwell equations in time-independent form are given by

$$\mathbf{E}(\mathbf{r}) = \nabla \times \mathbf{H}(\mathbf{r})/(-ik\varepsilon), \quad (7a)$$

$$\mathbf{H}(\mathbf{r}) = \nabla \times \mathbf{E}(\mathbf{r})/ik, \quad (7b)$$

where ε is permittivity, given by $\varepsilon = (m_r + im_i)^2$. We have chosen the time-harmonic factor as $\exp(ikct)$, in which c is the speed of light in vacuum. If this factor is selected as $\exp(-ikct)$, the sign of the imaginary part of the refractive index is negative.^{1,24} Using Eq. (7b), we can obtain the amplitude vectors of magnetic fields associated with the incident and reflected rays as follows:

$$\mathbf{H}_{io} = \hat{e}_i \times (E_{io,\alpha}\hat{\alpha}_i + E_{io,\beta}\hat{\beta}) = E_{io,\beta}\hat{\alpha}_i - E_{io,\alpha}\hat{\beta}, \quad (8a)$$

$$\mathbf{H}_{ro} = \hat{e}_r \times (E_{ro,\alpha}\hat{\alpha}_r + E_{ro,\beta}\hat{\beta}) = E_{ro,\beta}\hat{\alpha}_r - E_{ro,\alpha}\hat{\beta}. \quad (8b)$$

For the refractive wave in an absorbing medium, a transverse-wave condition cannot be imposed simultaneously on the electric and the magnetic fields because of the inhomogeneity effect; that is, the TEM wave mode is not valid in this case.

In the following discussion, first we examine the reflecting characteristics of an absorbing medium for various wave modes. To derive the reflection coefficient, we can assume that the electric field is transverse with respect to the propagation direction of the ray (hereafter this mode is referred to as the TE mode), so the refracted electric field can be expressed in the form

$$\mathbf{E}_{to} = E_{to,\alpha}\hat{\alpha}_t + E_{to,\beta}\hat{\beta}. \quad (9)$$

From Eqs. (1c), (4), (7b), and (9) and the relationship of $\hat{n} = \cos \zeta_t \hat{e}_t - \sin \zeta_t \hat{\alpha}_t$, the refracted magnetic field in the TE mode can be obtained as follows:

$$\begin{aligned} \mathbf{H}_{to}(\mathbf{r}) &= (N_r \hat{e}_t + iN_n \hat{n}) \times (E_{to,\alpha}\hat{\alpha}_t + E_{to,\beta}\hat{\beta}) \\ &= (N_r + iN_n)E_{to,\beta}\hat{\alpha}_t - (N_r + iN_n)E_{to,\alpha}\hat{\beta} \\ &\quad + iN_n \sin \zeta_t E_{to,\beta}\hat{e}_t. \end{aligned} \quad (10)$$

From Eq. (10) it is evident that the refracted magnetic field has a nonzero component along unit vector

\hat{e}_t (ray direction) when N_n is not zero, i.e., when absorption is involved. At the interface of two media, the electromagnetic boundary condition requires that the tangential components of electric and magnetic fields be continuous. Thus we have the following relationships:

$$E_{io,\beta} + E_{ro,\beta} = E_{to,\beta}, \quad (11a)$$

$$E_{io,\beta} \cos \zeta_i - E_{ro,\beta} \cos \zeta_i = [(N_r + iN_n) \cos \zeta_t + iN_n \sin^2 \zeta_t] E_{to,\beta}, \quad (11b)$$

$$E_{io,\alpha} + E_{ro,\alpha} = (N_r + iN_n) E_{to,\alpha}, \quad (11c)$$

$$E_{io,\alpha} \cos \zeta_i - E_{ro,\alpha} \cos \zeta_i = \cos \zeta_t E_{to,\alpha}. \quad (11d)$$

The preceding equations can be solved to yield the reflection coefficients for the two polarization configurations:

$$\begin{aligned} R_{TE,\perp} &= E_{ro,\beta}/E_{io,\beta} \\ &= \frac{\cos \zeta_i - [(N_r + iN_n) \cos \zeta_t + iN_n \sin^2 \zeta_t]}{\cos \zeta_i + [(N_r + iN_n) \cos \zeta_t + iN_n \sin^2 \zeta_t]} \\ &= \frac{\cos \zeta_i - (N_r \cos \zeta_t + iN_n)}{\cos \zeta_i + (N_r \cos \zeta_t + iN_n)}, \end{aligned} \quad (12a)$$

$$R_{TE,\parallel} = E_{ro,\alpha}/E_{io,\alpha} = \frac{(N_r + iN_n) \cos \zeta_i - \cos \zeta_t}{(N_r + iN_n) \cos \zeta_i + \cos \zeta_t}. \quad (12b)$$

Similarly, if we assume that the magnetic field of the refracted wave is transverse with respect to the ray direction (hereafter, this mode is referred to as the TM mode), the reflection coefficients are then given by

$$R_{TM,\perp} = \frac{(N_r + iN_n) \cos \zeta_i - \varepsilon \cos \zeta_t}{(N_r + iN_n) \cos \zeta_i + \varepsilon \cos \zeta_t}, \quad (13a)$$

$$R_{TM,\parallel} = \frac{\varepsilon \cos \zeta_i - (N_r \cos \zeta_t + iN_n)}{\varepsilon \cos \zeta_i + (N_r \cos \zeta_t + iN_n)}. \quad (13b)$$

Therefore, considering the two wave modes and two polarization configurations, four combinations are possible for the reflection coefficients: $(R_{TM,\parallel}, R_{TM,\perp})$, $(R_{TE,\parallel}, R_{TE,\perp})$, $(R_{TE,\parallel}, R_{TM,\perp})$, and $(R_{TM,\parallel}, R_{TE,\perp})$. Each of these four combinations is a mathematically rational solution derived from the electromagnetic boundary condition when an absorptive medium is involved. However, only one of the four solutions should be computationally correct in the ray-tracing calculation relative to the process of scattering an electromagnetic wave by a dielectric particle with absorption. It should be pointed out that the Maxwell equations, subject to the appropriate boundary conditions, always have a unique solution, as in the case of Mie theory. The explanation for the multiple solutions for the reflection coefficients is that the electromagnetic boundary condition is locally imposed within the context of geometrical optics, which permits treatment of the inhomogeneous refracted wave as a refracted ray, thereby providing

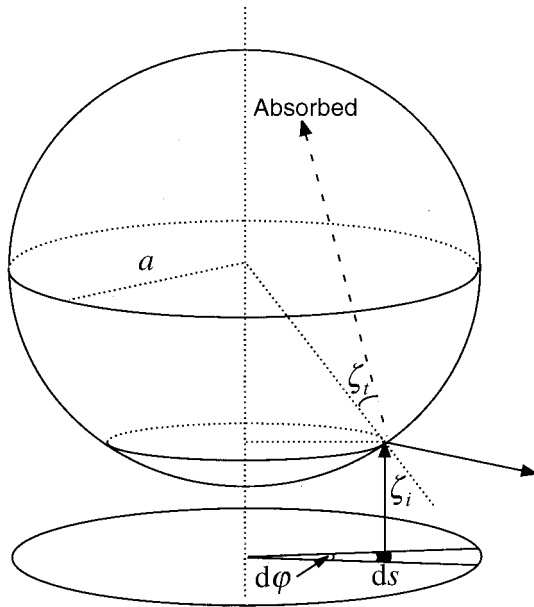


Fig. 2. Scattering geometry for a large sphere with strong absorption.

the basis for a ray-tracing procedure. Accordingly, we are looking for the pair of reflection coefficients that provide the best numerical agreement with the exact solution in scattering computation.

To identify the computationally correct pair of reflection coefficients from among the preceding four combinations, we consider the scattering geometry in Fig. 2 for a strongly absorptive sphere with a size much larger than incident wavelength. In this case the scattered field is composed primarily of the contributions from diffraction and external reflection. The incident energy associated with area element ds on the projected area is scattered in angular element $\sin \theta d\theta d\phi$ in which θ is the scattering angle. The scattered intensity at a distance r that is far from the particle is given by

$$I_s = I_0 \frac{|R|^2}{r^2} \left| \frac{ds}{\sin \theta d\theta d\phi} \right| = I_0 \frac{|R|^2 a^2}{4r^2}, \quad (14)$$

where a is the radius of the sphere; I_0 and I_s are incident and scattered intensities, respectively; R is a reflection coefficient without specification of a wave mode and polarization configuration. To derive Eq. (14) we used two relationships, $ds = a^2 \cos \zeta_i \sin \zeta_i d\zeta_i d\phi$ and $\theta = \pi - 2\zeta_i$. However, according to the definition of the scattering phase function denoted P , one can define the following relationship:

$$I_s = \frac{\sigma_s}{4\pi r^2} P I_0, \quad (15)$$

where σ_s is the scattering cross section. Therefore, after the two polarization configurations are accounted for, the contribution of the external reflection to the phase function can be obtained by a comparison of Eqs. (14) and (15):

$$\begin{aligned} P^r(\theta) &= \frac{1}{2} \frac{(|R_{\parallel}|^2 + |R_{\perp}|^2) \pi a^2}{\sigma_s} \\ &= \frac{1}{2} \frac{(|R_{\parallel}|^2 + |R_{\perp}|^2)}{Q_e - Q_a}, \end{aligned} \quad (16)$$

where Q_e and Q_a are the extinction efficiency and the absorption efficiency, respectively. The value of Q_e is 2 because the particle is very large, whereas Q_a is determined by the ratio of refracted energy to the incident energy associated with the projected area. Note that the divergence factor introduced by van de Hulst²⁵ is absent in Eq. (16) because the rays that are transmitted through the sphere are ignored here.

An improved diffraction formulation has been derived by Yang and Liou²⁶ that, unlike the conventional method that is limited to scattering angles smaller than 90° , can be applied to the entire scattering angular region. When the improved method is applied to the diffraction by a sphere, the scattering amplitude matrix²⁵ is given by

$$\begin{bmatrix} S_2 & S_3 \\ S_4 & S_1 \end{bmatrix} = \frac{(ka)^2 2J_1(ka \sin \theta)}{4 ka \sin \theta} \times \begin{bmatrix} \cos \theta(1 + \cos \theta) & 0 \\ 0 & 1 + \cos \theta \end{bmatrix}, \quad (17)$$

where J_1 is the Bessel function of the first kind. The phase function that includes the contribution from diffraction and external reflection can be obtained from Eqs. (16) and (17) as follows:

$$\begin{aligned} P(\theta) &= \frac{(ka)^2}{8(Q_e - Q_a)} \left[\frac{2J_1(ka \sin \theta)}{ka \sin \theta} \right]^2 \\ &\times (1 + \cos^2 \theta)(1 + \cos \theta)^2 + \frac{1}{2} \frac{(|R_{\parallel}|^2 + |R_{\perp}|^2)}{Q_e - Q_a}. \end{aligned} \quad (18)$$

In addition to the phase function, one should use the polarization configuration to identify the correct combination of reflection coefficients. When the incident radiation is unpolarized, the polarization feature of scattered radiation can be specified by the degree of linear polarization (DLP). When scattered radiation is composed of diffraction and external reflection, the DLP associated with the phase function in Eq. (18) can be given as follows:

$$\text{DLP}(\theta) = \frac{I_{\perp}^d(\theta) - I_{\parallel}^d(\theta) + I_{\perp}^r(\theta) - I_{\parallel}^r(\theta)}{I_{\perp}^d(\theta) + I_{\parallel}^d(\theta) + I_{\perp}^r(\theta) + I_{\parallel}^r(\theta)} = \frac{(ka)^2 [2J_1(ka \sin \theta)/ka \sin \theta]^2 (1 + \cos \theta)^2 (1 - \cos^2 \theta) + 4(|R_{\perp}|^2 - |R_{\parallel}|^2)}{(ka)^2 [2J_1(ka \sin \theta)/ka \sin \theta]^2 (1 + \cos \theta)^2 (1 + \cos^2 \theta) + 4(|R_{\perp}|^2 + |R_{\parallel}|^2)}, \quad (19)$$

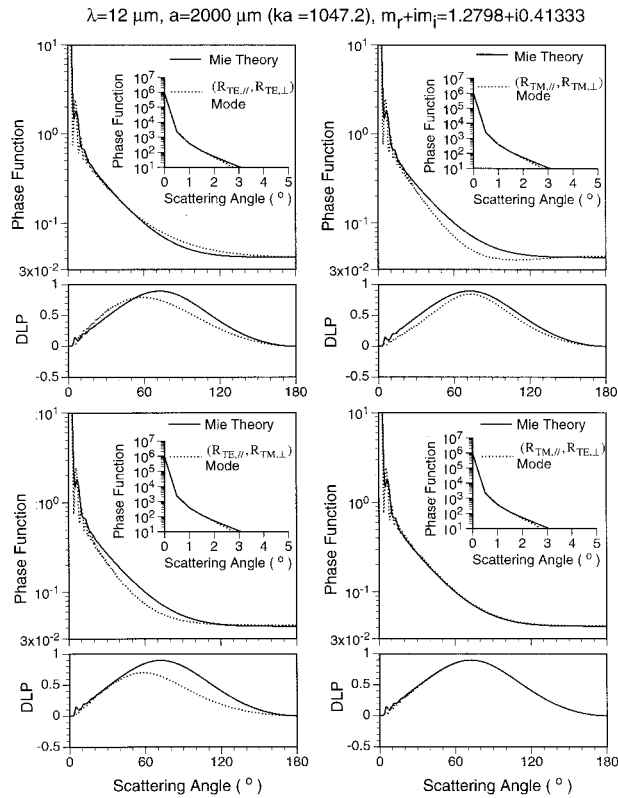


Fig. 3. Phase function and the degree of linear polarization computed from geometrical optics compared with the Mie solution at $\lambda = 12 \mu\text{m}$.

where I_{\perp}^d and I_{\perp}^r (I_{\parallel}^d and I_{\parallel}^r) are the scattered intensity associated with diffraction and external reflection, respectively, when the electric field is polarized along a direction that is perpendicular (parallel) to the scattering plane.

Figure 3 shows the phase function and the DLP computed from Mie theory and the geometrical-optics method at a wavelength of $12 \mu\text{m}$. The Mie computational code developed by Wiscombe²⁷ is used in this study. Because the size parameter is extremely large ($\chi = 1047.2$), the scattered energy at a large scattering angle (approximately 20° in this case) comes primarily from the reflection of incident rays. Through comparison of the geometrical-optics solution and the Mie results, we can identify the correct reflection coefficient pair. Evidently, the reflection coefficient pair ($R_{TM,\parallel}$, $R_{TE,\perp}$) produces a phase function and a DLP consistent with the Mie solution at large scattering angles, where the external reflection dominates. As the Mie solution for the DLP is positive for the entire scattering domain, the reflection of the incident wave with a vertical polarization configuration is much larger than the reflection when the polarization is parallel to the scattering plane. For this reason, if we incorrectly apply reflection coefficient $R_{TM,\perp}$ for the incident wave polarized perpendicularly with respect to scattering plane, substantial errors can result for both phase function and DLP, as is evident from Fig. 3.

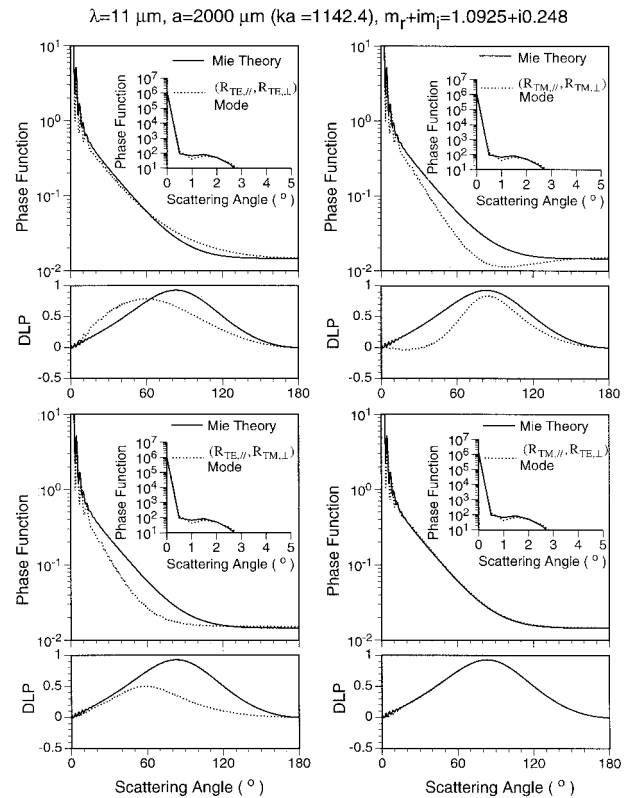


Fig. 4. The same as Fig. 3, except that here the wavelength is $11 \mu\text{m}$.

Figure 4 is similar to Fig. 3, except that the wavelength is $11 \mu\text{m}$ and the real part of the refractive index is close to unity (see Fig. 1). It can be seen that the phase function values at large scattering angles at $11 \mu\text{m}$ are much smaller than the corresponding results at $12 \mu\text{m}$ because external reflection is weaker for the former wavelength. However, the correctness of the reflection coefficients used in the computation is also critical to the phase function and the DLP, even in the optically tenuous case. As a matter of fact, the errors associated when the wrong wave mode is assumed for the refracted wave are even more pronounced for the results shown in Fig. 4 than for those shown in Fig. 3. From these results it is clear that the correct wave mode must be used for the refracted wave in the derivation of the reflection coefficients, regardless of the magnitude of the real part of the refractive index whenever the particle is strongly absorptive.

A comparison of the ray-tracing method and Mie theory for obtaining the phase function of spheres has been presented by Liou and Hansen²⁸ for a polydisperse case that has an assumed particle size distribution. For the monodisperse case (a system composed of particles that have a single size and shape), a comparison study has been presented by Macke *et al.*²⁹ for spheroids and finite circular cylinders at a near-infrared wavelength, which

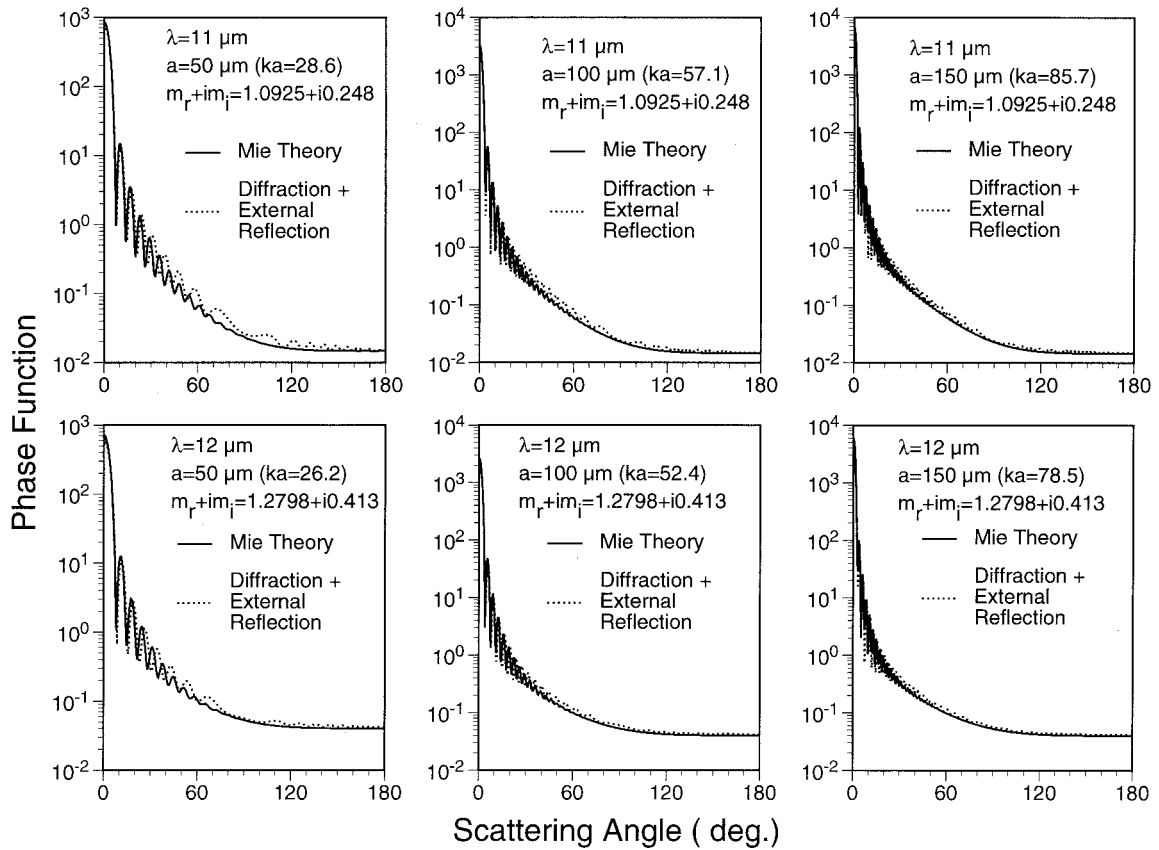


Fig. 5. Comparison of the phase functions computed from Mie theory and from the geometrical-optics method for three moderate sizes at wavelengths of 11 and 12 μm .

shows that the applicable size parameter for the geometrical-optics method is approximately 60. In addition, these authors²⁹ pointed out that the size parameter required for a convergence of the exact solution and the geometrical-optics solution is larger for spheres than for nonspherical particles.

The results of this study suggest that the geometrical-optics method can be applied to much smaller size parameters when strong absorption is involved. Figure 5 shows the phase function computed from Eq. (18) in comparison with the Mie solutions. Evidently, when the size parameter is larger than approximately 30, one can use the geometrical-optics solution to approximate the exact solution. For size parameters larger than 50, the geometrical-optics solution essentially converges to the exact solution in the side and backscattering directions.

From the preceding discussions associated with Figs. 3–5, it is clear that TM and TE modes should be applied to the components of electric fields that are parallel and perpendicular, respectively, to the incident plane. By using this combination of wave modes, one can straightforwardly derive the refracted wave on the basis of electromagnetic boundary conditions. Through application of the $(\text{TM}_{\parallel}, \text{TE}_{\perp})$ wave mode to the refracted

wave, we can obtain the refracted electric field as follows:

$$\mathbf{E}_{t,o} = E_{t,o,\alpha}\hat{\alpha}_t + E_{t,o,\beta}\hat{\beta} + E_{t,o,\gamma}\hat{e}_t, \quad (20a)$$

$$\begin{pmatrix} E_{t,o,\alpha} \\ E_{t,o,\beta} \\ E_{t,o,\gamma} \end{pmatrix} = \begin{bmatrix} T_{\alpha} & 0 \\ 0 & T_{\beta} \\ T_{\gamma} & 0 \end{bmatrix} \begin{pmatrix} E_{i,o,\alpha} \\ E_{i,o,\beta} \end{pmatrix}, \quad (20b)$$

where

$$T_{\alpha} = \frac{2(N_r + iN_i)\cos \zeta_i}{\epsilon \cos \zeta_i + (N_r \cos \zeta_t + iN_n)}, \quad (20c)$$

$$T_{\beta} = \frac{2 \cos \zeta_i}{\cos \zeta_i + (N_r \cos \zeta_t + iN_n)}, \quad (20d)$$

$$T_{\gamma} = \frac{i2N_n \sin \zeta_t \cos \zeta_i}{\epsilon \cos \zeta_i + (N_r \cos \zeta_t + iN_n)}. \quad (20e)$$

Note that in Eqs. (20) the dependence of these parameters on the wave mode is not specified explicitly. It should be pointed out that the transmission matrix in the conventional ray-tracing scheme is a 2×2 matrix. When absorption is involved, the transmission matrix becomes a 3×2 matrix. When absorption of the medium is absent, T_{γ} is reduced to zero because N_n is zero and Eqs. (20) are reduced to

the conventional Fresnel refraction coefficients.

3. Asymptotic Solution for Scattering and Absorption Properties of Large Polyhedral Particles with Strong Absorption

A. Physical Basis for the Asymptotic Solution

In Section 2 it was shown that the conventional geometrical-optics approach in terms of the superposition of diffraction and external reflection can well approximate the Mie solution for the spherical-particle case when the size parameter is large and the particle is absorptive. Because the variation in the surface normal direction is continuous for a sphere, a continuous distribution of the externally reflected energy is obtained. However, this is not true if the particle geometry is a polyhedron such as a hexagonal plate or column, which is the basic geometric structure of ice crystals in cirrus clouds. In the numerical solution, there is a physically incorrect discontinuous distribution of scattered energy for any specific orientation of the particle.

For example, consider the scattering of radiation by a hexagonal ice column when the incident radiation is perpendicular to the c axis of the particle and parallel to a line that connects two symmetric apexes of particle cross section. If the rays refracted into the particle are ignored because of absorption, the phase function can be written as follows:

$$P(\theta_s, \varphi_s) = \frac{3k^2 La}{8\pi\sigma_s} \left\{ \frac{\sin[(kL/2)\sin\theta_s \cos\varphi_s]}{(kL/2)\sin\theta_s \cos\varphi_s} \frac{\sin[(\sqrt{3}ka/2)\sin\theta_s \sin\varphi_s]}{(\sqrt{3}ka/2)\sin\theta_s \sin\varphi_s} \right\}^2 \times (1 + \cos^2\theta_s)(1 + \cos\theta_s)^2 + \frac{\sqrt{3}\pi aL}{\sigma_s} [\delta(\varphi_s - \pi/2) + \delta(\varphi_s + \pi/2)]\delta(\theta_s - 2\pi/3)[|R_{TM,\parallel,\zeta_i=\pi/6}|^2 + |R_{TE,\perp,\zeta_i=\pi/6}|^2], \quad (21a)$$

$$\sigma_s = \sqrt{3}aL(2 - |R_{TM,\parallel,\zeta_i=\pi/6}|^2 - |R_{TE,\perp,\zeta_i=\pi/6}|^2), \quad (21b)$$

where L and a are the length and the semiwidth, respectively, of the hexagonal columns and $\delta(x)$ is the Dirac delta function. To avoid any possible confusion, in Eqs. (21) we use θ_s to indicate the scattering angle and φ_s for the azimuthal angle of the scattering plane. Here the plane of $\varphi_s = 0^\circ$ is the plane that contains the incident direction and the c axis of the particle. On the right-hand side of Eq. (21a), the first term represents the contribution from diffraction and the second term represents the contribution from external reflection. Obviously, the second term is nonzero at only two angles, as is expressed by the delta functions. This singularity is inherent in the

conventional geometrical-optics method. The delta reflection involved in Eqs. (21) originates from the same physical mechanism of the forward delta transmission that has been well explained by Takano and Liou¹² and Mishchenko and Macke.³⁰ It should be pointed out that the singularity in Eq. (21b) could be overcome numerically in the ray-tracing calculation if the particles were randomly oriented in space. The average intensity is given by the scattered energy divided by the corresponding solid angle elements. The discontinuity could be avoided, given proper resolution for the solid angle elements with sufficient orientations of the particles, i.e., with sufficiently random orientation.

To circumvent this particular disadvantage of the conventional method for a specific orientation, we apply the geometrical-optics method to solve for the internal field inside the particle, following Yang and Liou.³¹ The scattered far-field, extinction, and absorption cross sections are given by

$$\mathbf{E}^s(\mathbf{r}) = \frac{k^2 \exp(ikr)}{4\pi r} (\epsilon - 1) \iiint_{\nu} \{\mathbf{E}(\mathbf{r}') - \hat{r}[\hat{r} \cdot \mathbf{E}(\mathbf{r}')]\} \times \exp(-ik\hat{r} \cdot \mathbf{r}') d^3r', \quad (22a)$$

$$\sigma_{\text{ext}} = \text{Im} \left[\frac{k}{|\mathbf{E}_i|} (\epsilon - 1) \iiint_{\nu} \mathbf{E}(\mathbf{r}') \mathbf{E}_i(\mathbf{r}') d^3r' \right], \quad (22b)$$

$$\sigma_{\text{abs}} = \frac{k}{|\mathbf{E}_i|^2} \epsilon_i \iiint_{\nu} \mathbf{E}(\mathbf{r}') \cdot \mathbf{E}_i(\mathbf{r}') d^3r', \quad (22c)$$

respectively. The integrals involved in Eqs. (22) can be calculated by use of the ray-by-ray integration algorithm.³¹ From the ray-by-ray integration calculation and Eqs. (22), the amplitude scattering matrix and the extinction and absorption cross sections are given by

$$\begin{bmatrix} S_2(\hat{e}_s) & S_3(\hat{e}_s) \\ S_4(\hat{e}_s) & S_1(\hat{e}_s) \end{bmatrix} = \frac{k^2(\epsilon - 1)}{4\pi} \iint_{\text{surface}} \frac{\cos\zeta_i}{N_r + iN_i - \hat{e}_s \cdot \hat{e}_t} \begin{bmatrix} \hat{\alpha}_s \cdot \hat{\alpha}_t & \hat{\alpha}_s \cdot \hat{\beta} & \hat{\alpha}_s \cdot \hat{e}_s \\ \hat{\beta}_s \cdot \hat{\alpha}_t & \hat{\beta}_s \cdot \hat{\beta} & \hat{\beta}_s \cdot \hat{e}_s \end{bmatrix} \begin{bmatrix} T_\alpha & 0 \\ 0 & T_\beta \\ T_\gamma & 0 \end{bmatrix} \begin{bmatrix} \hat{\alpha}_i \cdot \hat{\alpha}_0 & \hat{\alpha}_i \cdot \hat{\beta}_s \\ \hat{\beta} \cdot \hat{\alpha}_0 & \hat{\beta} \cdot \hat{\beta}_s \end{bmatrix} \times \exp[-ik(\hat{e}_i - \hat{e}_s) \cdot \mathbf{r}'] [1 - \exp[-kN_i l(\mathbf{r}')] \exp[ik(N_r - \hat{e}_s \cdot \hat{e}_t) l(\mathbf{r}')]] d^2r', \quad (23a)$$

$$\sigma_{\text{ext}} = \frac{2\pi}{k^2} \text{Re}[S_1(\hat{e}_i) + S_2(\hat{e}_i)], \quad (23b)$$

$$\sigma_{\text{abs}} = \frac{1}{2} \iint_{\text{particle surface}} \cos \zeta_i N_r (|T_\alpha|^2 + |T_\beta|^2 + |T_\gamma|^2) \times \{1 - \exp[-2kN_i l(r')]\} d^2r', \quad (23c)$$

where $\hat{\beta}_s$ is a unit vector perpendicular to the scattering plane, \hat{e}_s is along the scattering direction, $\hat{\alpha}_s = \hat{e}_s \times \hat{\beta}_s$, $\hat{\alpha}_o = \hat{e}_i \times \hat{\beta}_s$, and $l(\mathbf{r}')$ is the ray penetration depth with the incident point at \mathbf{r}' . The other variables involved were defined above. If the absorbing particle is large, it is expected that $\exp[-kN_i l(\mathbf{r}')] \rightarrow 0$. In this case, analytical expressions can be derived for the integrations involved in Eqs. (23a) and (23c) if the surface of the particle is locally flat, as in the case of polyhedral geometry.

For a given flat face of the particle surface, Fresnel reflection does not vary with the location at the face because the incident angles are the same for all the points on this face. Thus the following matrix is independent of the position of a point on a flat surface:

$$\begin{bmatrix} \tilde{S}_2 & \tilde{S}_3 \\ \tilde{S}_4 & \tilde{S}_1 \end{bmatrix}_j = \frac{\cos \zeta_i}{N_r + iN_i - \hat{e}_s \cdot \hat{e}_i} \begin{bmatrix} \hat{\alpha}_s \cdot \hat{\alpha}_i & \hat{\alpha}_s \cdot \hat{\beta} & \hat{\alpha}_s \cdot \hat{e}_s \\ \hat{\beta}_s \cdot \hat{\alpha}_i & \hat{\beta}_s \cdot \hat{\beta} & \hat{\beta}_s \cdot \hat{e}_s \end{bmatrix} \times \begin{bmatrix} T_\alpha & 0 \\ 0 & T_\beta \\ T_\gamma & 0 \end{bmatrix} \begin{bmatrix} \hat{\alpha}_i \cdot \hat{\alpha}_o & \hat{\alpha}_i \cdot \hat{\beta}_s \\ \hat{\beta}_i \cdot \hat{\alpha}_o & \hat{\beta}_i \cdot \hat{\beta}_s \end{bmatrix}. \quad (24)$$

Therefore, the integral in Eq. (23a) should actually be evaluated only with respect to the phase variation over the local flat faces of the particle. For purposes of evaluation the surface of a polyhedral particle can be divided into a number of area elements shaped as parallelograms and triangles. For a parallelogram or a triangular face, the position vector of a point on this face is expressed by

$$\mathbf{r} = \begin{cases} \mathbf{r}_0 + \xi \mathbf{r}_1 + \eta \mathbf{r}_2 & \text{parallelogram} \\ \mathbf{r}_0 + \xi(1 - \eta) \mathbf{r}_1 + \eta \xi \mathbf{r}_2 & \text{triangle} \end{cases}, \quad (25)$$

where \mathbf{r}_0 is the position vector of the apex of the geometric shape and \mathbf{r}_1 and \mathbf{r}_2 constitute the neighboring two sides of the shape. $\xi \in [0,1]$ and $\eta \in [0,1]$. From Eqs. (24) and (25), the integration of phase variation over a parallelogram area element yields

$$\begin{aligned} D_i &= \iint_{\text{face } j} \exp\{ik(\hat{e}_i - \hat{e}_s) \cdot \mathbf{r}_j\} d^2\mathbf{r}_j \\ &= |\mathbf{r}_{j,1} \times \mathbf{r}_{j,2}| \int_0^1 \int_0^1 \exp\{ik(\hat{e}_i - \hat{e}_s)(\mathbf{r}_{j,0} + \eta \mathbf{r}_{j,1} \\ &\quad + \xi \mathbf{r}_{j,2})\} d\eta d\xi \end{aligned}$$

$$\begin{aligned} &= |\mathbf{r}_{j,1} \times \mathbf{r}_{j,2}| \exp\{ik(\hat{e}_i - \hat{e}_s) \cdot (\mathbf{r}_{j,0} + \mathbf{r}_{j,1}/2 + \mathbf{r}_{j,2}/2)\} \\ &\quad \times \frac{\sin[k(\hat{e}_i - \hat{e}_s) \cdot \mathbf{r}_{j,1}/2]}{k(\hat{e}_i - \hat{e}_s) \cdot \mathbf{r}_{j,1}/2} \frac{\sin[k(\hat{e}_i - \hat{e}_s) \cdot \mathbf{r}_{j,2}/2]}{k(\hat{e}_i - \hat{e}_s) \cdot \mathbf{r}_{j,2}/2}. \end{aligned} \quad (26a)$$

Similarly, if the phase variation is integrated over a triangular area, it follows that

$$\begin{aligned} D_i &= \iint_{\text{face } j} \exp\{ik(\hat{e}_i - \hat{e}_s) \cdot \mathbf{r}_j\} d^2\mathbf{r}_j \\ &= |\mathbf{r}_{j,1} \times \mathbf{r}_{j,2}| \frac{\exp\{ik(\hat{e}_i - \hat{e}_s) \cdot \mathbf{r}_{j,0}\}}{ik(\hat{e}_i - \hat{e}_s) \cdot (\mathbf{r}_{j,2} - \mathbf{r}_{j,1})} \times \left\{ \exp\{ik(\hat{e}_i \right. \\ &\quad \left. - \hat{e}_s) \cdot \mathbf{r}_{j,2}/2\} \frac{\sin[k(\hat{e}_i - \hat{e}_s) \cdot \mathbf{r}_{j,2}/2]}{k(\hat{e}_i - \hat{e}_s) \cdot \mathbf{r}_{j,2}/2} - \exp\{ik(\hat{e}_i \right. \\ &\quad \left. - \hat{e}_s) \cdot \mathbf{r}_{j,1}/2\} \frac{\sin[k(\hat{e}_i - \hat{e}_s) \cdot \mathbf{r}_{j,1}/2]}{k(\hat{e}_i - \hat{e}_s) \cdot \mathbf{r}_{j,1}/2} \right\}. \end{aligned} \quad (26b)$$

The scattering matrix that includes the contribution from all the faces can be written as

$$\begin{bmatrix} S_2(\hat{e}_s) & S_3(\hat{e}_s) \\ S_4(\hat{e}_s) & S_1(\hat{e}_s) \end{bmatrix} = \frac{k^2(\epsilon - 1)}{4\pi} \sum_j h(\hat{e}_i \cdot \hat{n}_j) \times D_j \begin{bmatrix} \tilde{S}_2(\hat{e}_s) & \tilde{S}_3(\hat{e}_s) \\ \tilde{S}_4(\hat{e}_s) & \tilde{S}_1(\hat{e}_s) \end{bmatrix}_j, \quad (27)$$

where $h(\hat{e}_i \cdot \hat{n}_j)$ is a step function that indicates whether the face is illuminated by incident radiation:

$$h(\hat{e}_i \cdot \hat{n}_j) = \begin{cases} 1 & \hat{e}_i \cdot \hat{n}_j > 0 \\ 0 & \hat{e}_i \cdot \hat{n}_j \leq 0 \end{cases}. \quad (28)$$

Once the amplitude scattering matrix is given, the calculation of the phase function is straightforward on the basis of the definition presented by van de Hulst.²⁵ It should be pointed out that a special form of Eq. (27) is given here for a hexagonal particle without incorporation of the inhomogeneity effect of the refracted wave on the transmission matrix.³¹ The result presented in this study is more general and can be applied to any polyhedron with strong absorption.

Inasmuch as the multiple scattering calculation is based on the solution of the radiative transfer equation, the most important parameter of concern is the single-scattering albedo rather than the extinction or absorption cross section. In particular, in remote-sensing applications a predescribed optical thickness is usually used in the calculation of look-up tables for the microphysical or optical properties of cloud particles. For this reason, in the present calculation we focus on the phase function and the single-scattering albedo. The latter parameter is defined as

$$\tilde{\omega} = \frac{\sigma_{\text{ext}} - \sigma_{\text{abs}}}{\sigma_{\text{ext}}}, \quad (29)$$

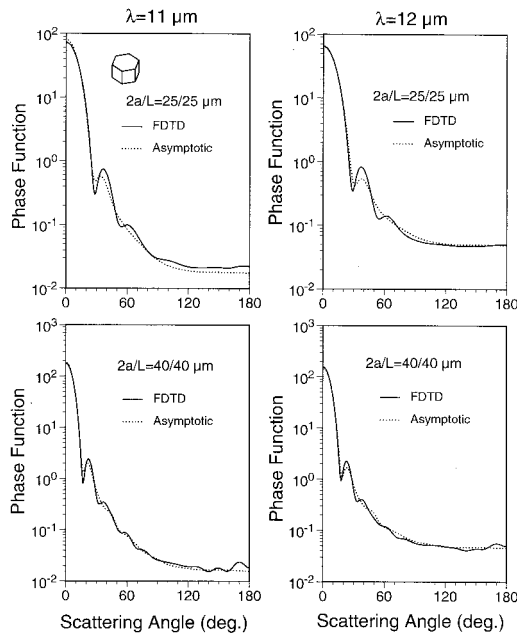


Fig. 6. Comparison of the phase function computed from the FDTD technique and from the present asymptotic theory for hexagonal ice crystals.

where the extinction and absorption cross sections, σ_{ext} and σ_{abs} , respectively, can be calculated from Eqs. (23b) and (23c).

B. Numerical Results for Hexagonal Ice Plates and Columns

As an application for the asymptotic solution for light scattering by a strongly absorptive particle, we present numerical results for ice crystals composed of hexagonal plates and solid columns. A hexagonal shape is selected here because this shape has been studied extensively for inference of cloud optical thickness and particle size in remote-sensing applications (see, e.g., Minnis *et al.*,³² Baum *et al.*,³³ and Han *et al.*³⁴).

Figure 6 shows a comparison of phase functions computed by the FDTD method and by the asymptotic theory [Eq. (27)] for hexagonal ice crystals of two sizes: $2a/L = 25 \mu\text{m}/25 \mu\text{m}$ and $2a/L = 40 \mu\text{m}/40 \mu\text{m}$, where L and a are the length and the semiwidth, respectively, of the hexagonal crystal. A random orientation condition is assumed for ice crystals in both the asymptotic and the FDTD calculations. It can be seen from Fig. 6 that the asymptotic solution more closely approximates the FDTD results for the larger particle size of $40/40 \mu\text{m}$. Although one might infer that the asymptotic theory can be applied to hexagonal ice crystals with sizes larger than approximately $40 \mu\text{m}$ in the infrared window region, the convergence between the FDTD and the asymptotic theories will, in fact, depend on the magnitude of absorption. For large particles at infrared wavelengths, the FDTD calculation is computationally expensive. Thus the asymptotic theory provides an efficient way to estimate the phase function of a large

particle with strong absorption. This advantage of the asymptotic theory in the calculation of the phase function is useful in practice. For example, the parameterization of cloud long-wave radiative properties requires that the phase function information be obtained through the use of either an asymmetry factor or a scaling factor,³⁵ which can be provided by

the asymptotic theory efficiently and accurately when the particle size is larger than approximately 40 μm .

Figure 7 shows a comparison of the single-scattering albedo computed from the FDTD and the asymptotic theories. In the figure, the results computed for the equivalent spheres are also shown. Following Mitchell *et al.*,³⁶ Fu *et al.*,³⁷ and Grenfell and Warren,³⁸ we define the radius of the equivalent sphere for a hexagonal particle as follows:

$$r_e = \frac{3V}{4A} = \frac{3}{2} \frac{\sqrt{3}/2aL}{\sqrt{3}/2a + L}, \quad (30)$$

where V is the volume of nonspherical particles and A is the projected area. Because strong absorption is assumed in the computation of the single-scattering albedo in the asymptotic theory, the result does not change with the variation of particle size. As a result, the asymptotic theory can lead to substantial errors in the single-scattering albedo calculation for small and moderate particle sizes. However, from the trend of the FDTD solution, it is expected that convergence between the FDTD and asymptotic results can be reached when the particle size is of the order of 200. Approaches developed by Fu *et al.*,³⁷ Mitchell,³⁹ and Baran and Havemann⁴⁰ can be used to overcome the shortcomings of the asymptotic theory in calculating single-scattering albedo. It

should be pointed out that these approaches cannot provide the information for the phase function. For this reason, a combination of these approaches (for the computation of single-scattering albedo) with the asymptotic theory (for the computation of phase function) would be more useful in practice.

Figures 8 and 9 show the phase functions of randomly oriented ice columns and plates in comparison with the phase functions of equivalent spheres. At large scattering angles, the phase function values are essentially the same for the spherical and the nonspherical particles. The external reflection becomes insensitive to particle geometry once the random orientation condition is assumed. However, for moderate particle sizes ($r_e = 26.7 \mu\text{m}$), substantial differences can be noted for the phase function at scattering angles in the 10–60° region for the two particle shapes.

Figure 10 shows the variation of the single-scattering albedo of hexagonal ice plates and columns that are randomly oriented in the infrared region from 8 to 16 μm . Also shown are the real and imaginary parts of refractive-index data compiled by Warren.⁴¹ Evidently, the variational pattern of the single-scattering albedo follows that of the real part of the refractive index. As we have mentioned, the real part of the refractive index has a value close to unity in the vicinity of 11 μm , and the corresponding

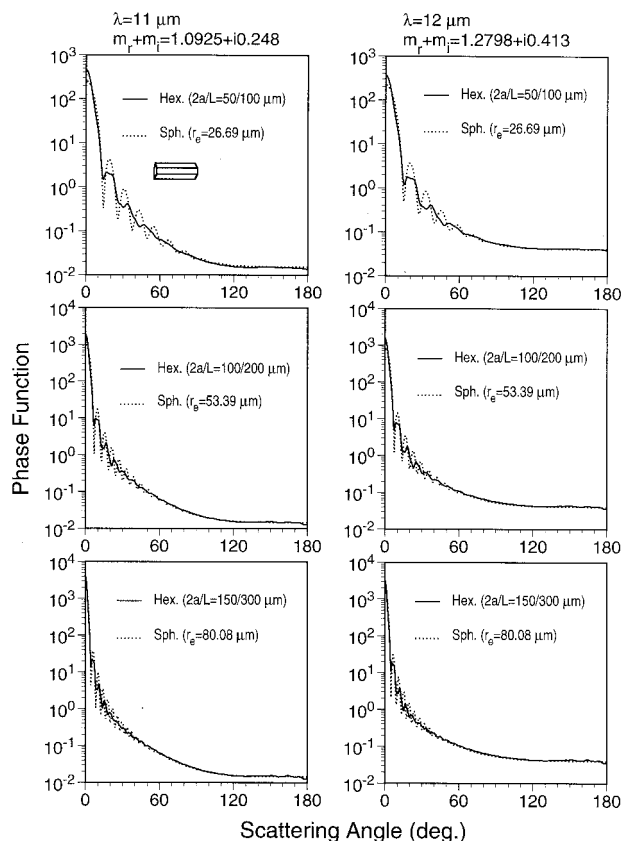


Fig. 8. Comparison of the phase function of hexagonal columns with that of equivalent spheres.

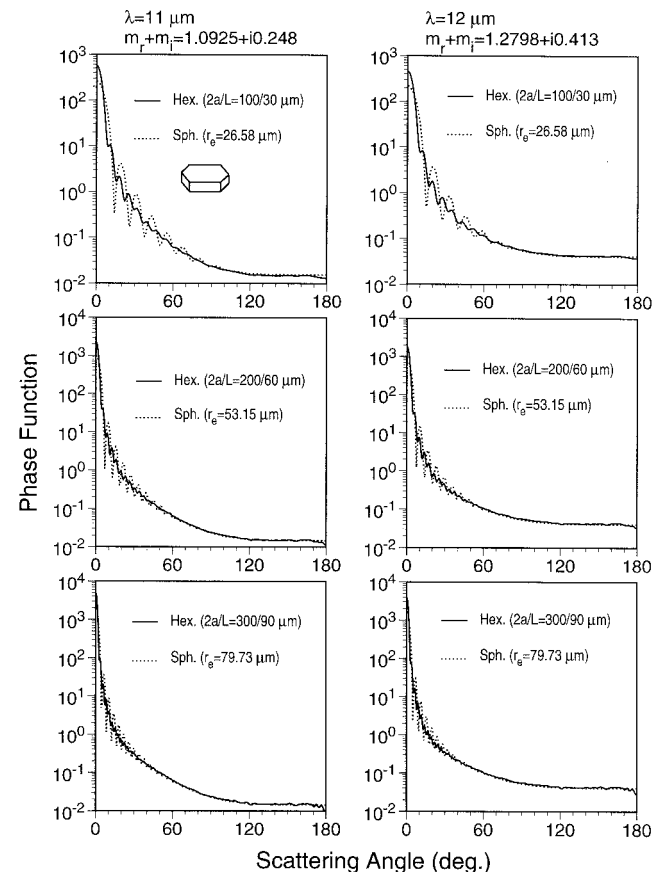


Fig. 9. As for Fig. 8 but for hexagonal plates.

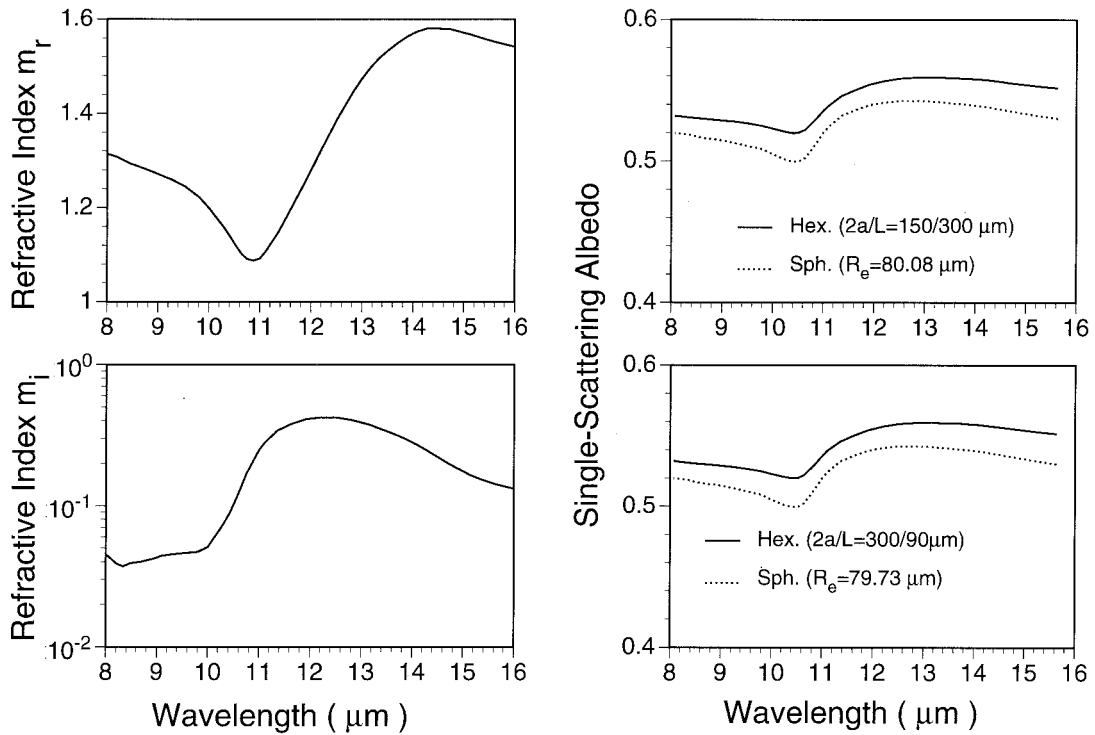


Fig. 10. Comparison of the single-scattering albedo values computed for hexagonal ice crystals and equivalent spheres.

imaginary part is substantially large. Near $11 \mu\text{m}$, the extinction of incident radiation is dominated by absorption and is known as the Christiansen effect.²³ As a result, a minimum is noted in the single-scattering albedo. From Fig. 10 it can also be seen that the single-scattering albedo for hexagonal par-

ticles is larger than for spheres. This property has been noted in a comparison of the FDTD solution with the equivalent spherical results that are shown in Fig. 7.

It is a common practice to assume that ice crystals are randomly oriented in space. However, in the

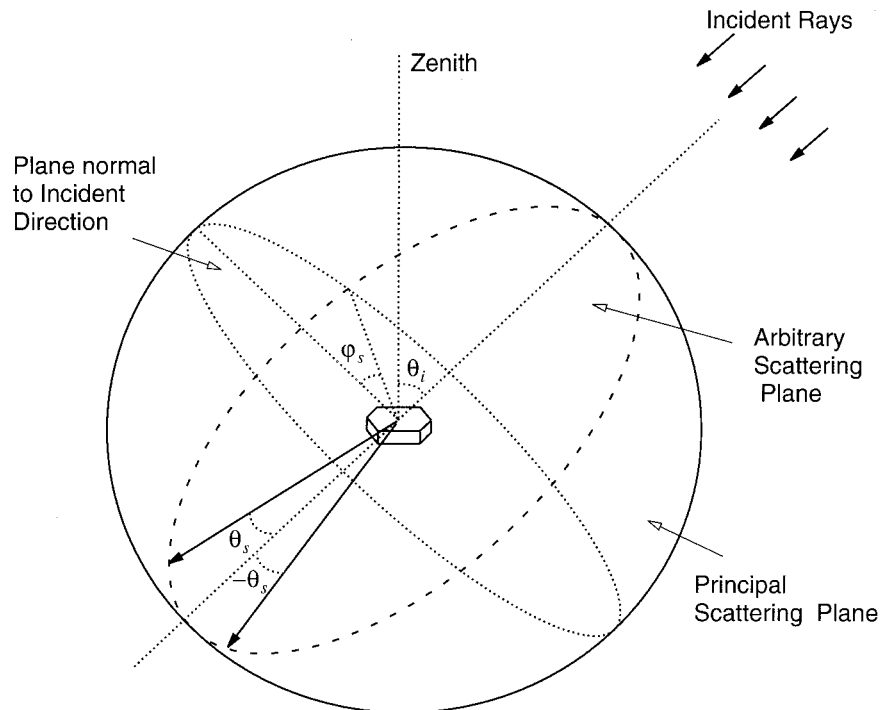


Fig. 11. Incident and scattering geometries for an ice crystal with preferred orientation.

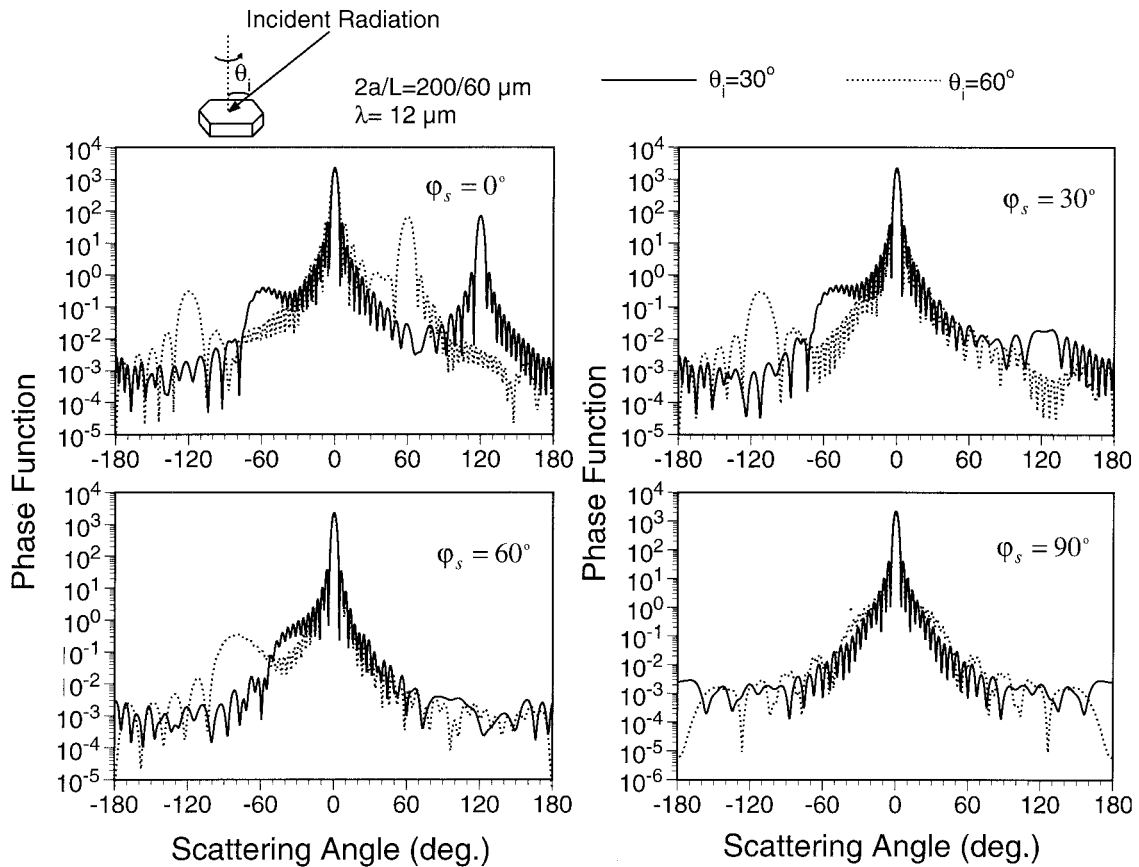


Fig. 12. Phase functions computed for hexagonal plates with preferred orientations.

atmosphere specific orientations are preferred for large plates and columns. For plates in an environment of a low Reynolds number, such as in a typical mid-latitude cirrus cloud, the a axis (the hexagonal asymmetric axis) of the particle tends to face vertically, whereas the c axis tends to be oriented horizontally. In other words, the crystals tend to align themselves so as to reach a stable state in the crystal falling process. The effect of preferred particle orientation on the phase function at visible wavelengths has been discussed by Takano and Liou⁴² and Rockwitz.⁴³ As we pointed out in Subsection 3.A, the application of a conventional ray-tracing technique will produce a discontinuity of the scattered energy and consequently cannot produce a continuous phase function. This shortcoming is avoided with the present analytical asymptotic theory. When preferred orientations are assumed for ice crystals, the phase function depends not only on the scattering angle but also on the scattering azimuthal angle, i.e., on which scattering plane the scattered field is observed. Figure 11 shows the geometry for the scattering configuration related to a plate oriented with its c axis aligned vertically. The principal plane ($\phi_s = 0^\circ$) is defined as the plane that contains the incident and the zenith directions. The plane that is normal to the incident direction is denoted by the dotted ellipse, whereas an arbitrary scattering plane is denoted by the dashed ellipse. On a given scat-

tering plane the positive scattering angle is measured, with a view along the incident direction, clockwise from the principal plane. For example, on the principal plane the scattering angle is positive if it is measured from the forward-scattering direction to the vertical zenith, whereas the scattering angle is negative if it is measured from the forward-scattering direction to the nadir view.

Figure 12 shows the phase function for hexagonal plates that have a preferred orientation for four scattering azimuthal angles. Ice crystals are rotated randomly about their c axes. The strong forward peak caused by diffraction can be seen for the four cases with different scattering azimuthal angles. For $\phi_s = 0^\circ$, very strong scattering peaks can be seen at scattering angles of 120° and 60° for incident zenith angles of 30° and 60° , respectively. The scattering maxima at 120° and 60° correspond to the specular reflection from the top faces of the plates. For $\phi_s = 0^\circ, 30^\circ, 60^\circ$, significant asymmetry in the phase function is observed in the scattering-angle regions of $(0^\circ, 180^\circ)$ and $(-0^\circ, -180^\circ)$. However, symmetry is observed for $\phi_s = 90^\circ$, as is expected. For plates with a preferred orientation, there are a number of ripple structures in the phase function that are caused by phase interference.

Figure 13 shows the phase function for ice columns with preferred orientations. The columns, randomly rotating about the zenith direction, are hori-

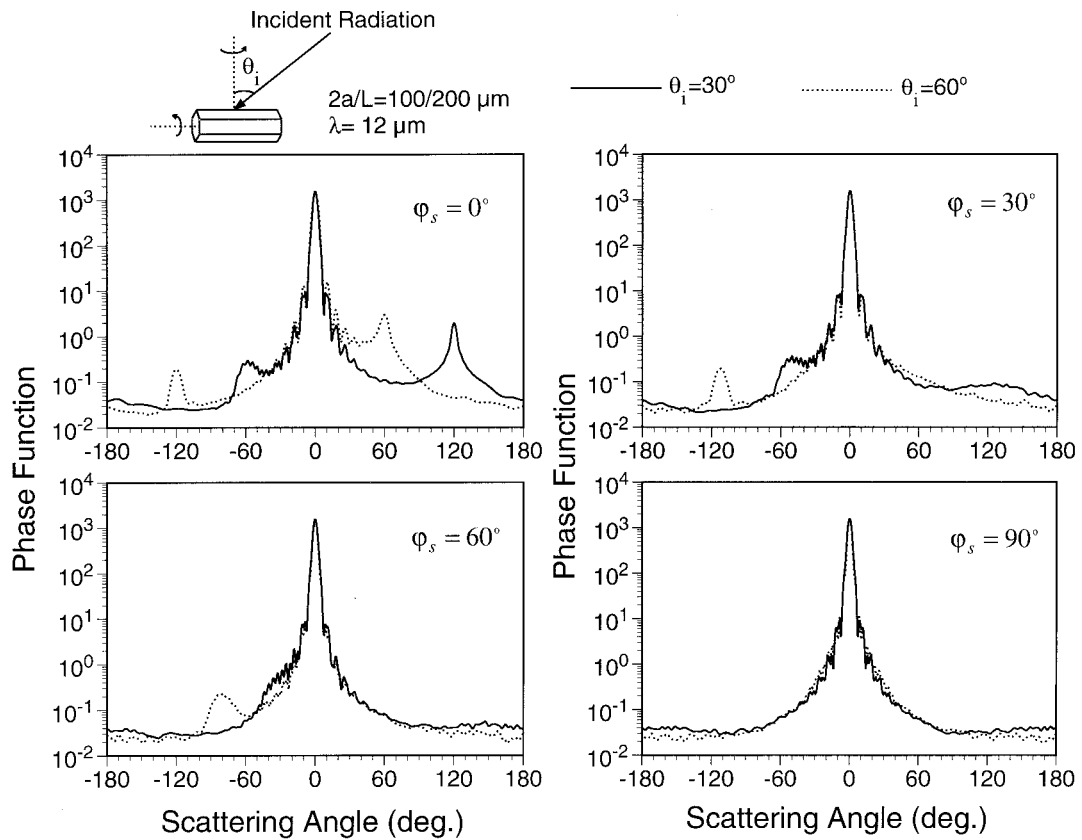


Fig. 13. As for Fig. 12 but for columns.

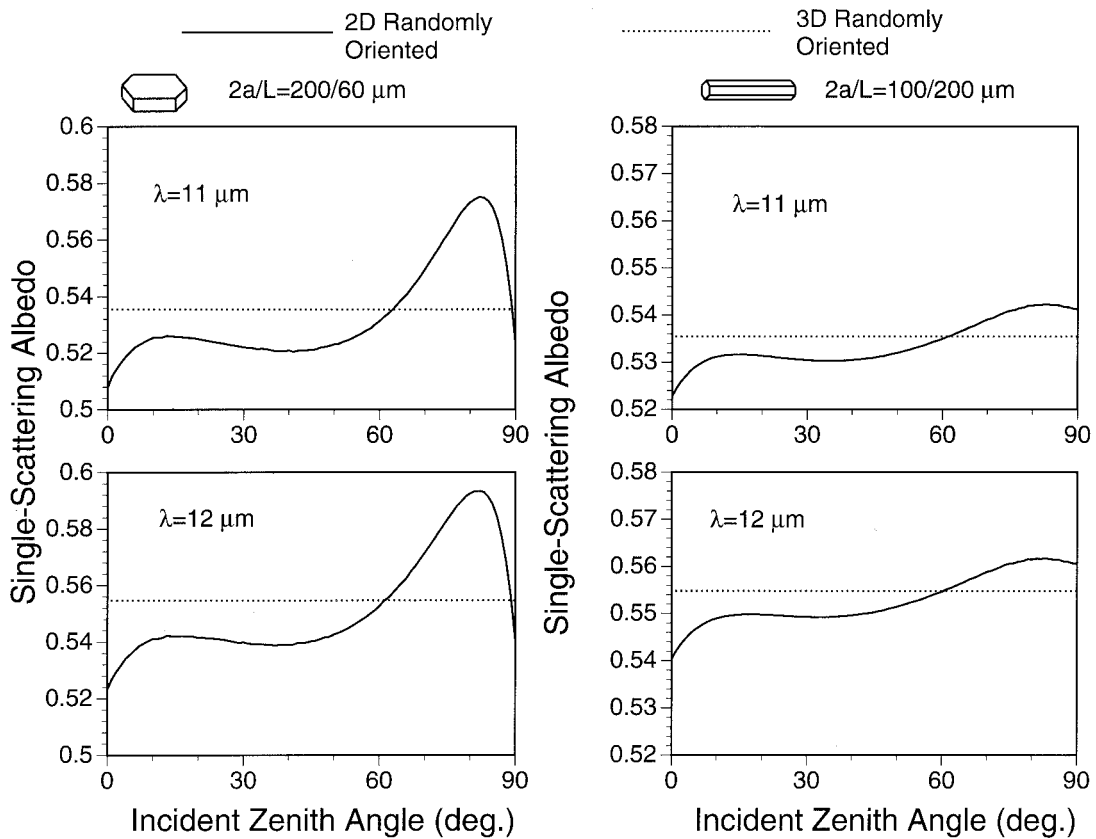


Fig. 14. Single-scattering albedo for ice crystals that have preferred orientations compared with the results for randomly oriented crystals.

zontally oriented but rotate randomly about their c axes. The ripple structure of plates caused by the phase interference as noted for Fig. 12 is largely smoothed out for oriented columns because the orientation of the particles in columns is more random. As for plates, the specular reflection feature is apparent when $\varphi_s = 0^\circ$.

Figure 14 shows the single-scattering albedo that corresponds to the phase functions in Figs. 12 and 13. Compared with the results for randomly oriented particles, the single scattering for both oriented plates and columns is smaller if the incident zenith angle is less than approximately 60° . For plates, there is a pronounced peak in the single-scattering albedo at the incident zenith of 70° . This peak is thought to be due to the external reflection for the top face of the plate that is increasing with increasing incident zenith angle. However, when this angle approaches 90° , the projected area of the top face is essentially zero, and the external reflection from the side faces, along with diffraction, dominates the scattered field.

4. Summary and Conclusions

An asymptotic solution in an analytical format for deriving the scattering properties of a general polyhedral particle with strong absorption has been presented. For scattering calculations involving nonspherical particles such as aerosols and ice crystals, we showed that the transverse-wave condition is not applicable to the refracted electromagnetic wave when absorption is involved. In the geometrical-optics solution for wave propagation in an absorbing dielectric medium, either the TM wave condition (i.e., when the magnetic field of the refracted wave is transverse to the wave direction) or the TE wave condition (i.e., when the electric field is transverse to the propagating direction of the wave) can be assumed for the refracted wave to satisfy the electromagnetic boundary condition. The wave mode assumed for the refracted wave affects both reflection and refraction coefficients. As a result, a nonunique solution for these coefficients is derived from the electromagnetic boundary condition. Through comparison of the asymptotic geometrical-optics solution and results determined from Mie theory for absorbing spheres, it has been shown that TM and TE wave modes should be applied to two polarized components that are parallel and perpendicular, respectively, to the incident plane. In this study we have identified the appropriate solution for the Fresnel reflection coefficients in the ray-tracing calculation. We presented the 3×2 refraction or transmission matrix that completely accounts for the inhomogeneity of the refracted wave in an absorbing medium. Based on the Fresnel coefficients for an absorbing medium, we derived the asymptotic solution in an analytical format for the scattering properties of a general polyhedral particle. Numerical results were presented for hexagonal plates and columns with both preferred and random orientation. The asymptotic theory produces reasonable accuracy in the phase function

calculations in the infrared window region (wavelengths near $10 \mu\text{m}$) if the particle size is of the order of $40\text{-}\mu\text{m}$ diameter or larger.

However, because strong absorption is assumed in the computation of the single-scattering albedo in the asymptotic theory, the single-scattering albedo does not change with variation of the particle size. As a result, the asymptotic theory can lead to substantial errors in the computation of single-scattering albedo for small and moderate particle sizes. However, from a comparison of results with the FDTD solution it is expected that a convergence between the FDTD results and the asymptotic theory results will be reached when the particle size approaches $200 \mu\text{m}$.

For two infrared wavelengths, 11 and $12 \mu\text{m}$, we showed that the phase function at side-scattering and backscattering angles is insensitive to particle shape if random orientation is assumed. For preferred orientations, however, we showed that the phase functions for plates and columns are significantly different. Additionally, when a preferred two-dimensional orientation condition is assumed, the phase function is observed to have a strong dependence on the scattering azimuthal angle. Moreover, numerical results show that the single-scattering albedo has a strong dependence on the inclination angle of incident radiation with respect to the rotating axis for the preferred particle orientations.

This research has been supported by a grant from NASA's MODIS project and partially by the U.S. Office of Naval Research and the Atmospheric Radiation Measurement program sponsored by the U.S. Department of Energy under contract DE-AI02-00ER62901.

References

1. M. I. Mishchenko, J. W. Hovenier, and L. D. Travis, *Light Scattering by Nonspherical Particles: Theory, Measurements, and Applications* (Academic, San Diego, Calif., 1999).
2. E. M. Purcell and C. R. Pennypacker, "Scattering and absorption of light by nonspherical dielectric grains," *Astrophys. J.* **186**, 705–714 (1973).
3. B. T. Draine and P. J. Flatau, "Discrete-dipole approximation for light calculations," *J. Opt. Soc. Am. A* **11**, 1491–1499 (1994).
4. P. Yang and K. N. Liou, "Finite-difference time domain method for light scattering by small ice crystals in three-dimensional space," *J. Opt. Soc. Am. A* **13**, 2072–2085 (1996).
5. W.-B. Sun, Q. Fu, and Z. Chen, "Finite-difference time-domain solution of light scattering by dielectric particles with a perfectly matched layer absorbing boundary condition," *Appl. Opt.* **38**, 3141–3151 (1999).
6. G. Mie, "Beitrage zur Optik truber Medien, speziell kolloidaler Metallosungen," *Ann. Phys. (Leipzig)* **25**, 377–445 (1908).
7. S. Asano and M. Sato, "Light scattering by randomly oriented spheroidal particles," *Appl. Opt.* **19**, 962–974 (1980).
8. V. G. Farafonov, N. V. Voshchinnikov, and V. V. Somsikov, "Light scattering by a core-mantle spheroidal particle," *Appl. Opt.* **35**, 5412–5426 (1996).
9. M. I. Mishchenko, "Light scattering by randomly oriented axially symmetric particles," *J. Opt. Soc. Am. A* **8**, 871–882 (1991).
10. M. I. Mishchenko, "Light scattering by size-shape distributions of randomly oriented axially symmetric particles of a size comparable to a wavelength," *Appl. Opt.* **32**, 623–625 (1993).

11. M. I. Mishchenko and A. Macke, "How big should hexagonal ice crystals be to produce halos?" *Appl. Opt.* **38**, 1626–1629 (1999).
12. Y. Takano and K. N. Liou, "Solar radiative transfer in cirrus clouds. I. Single-scattering and optical properties of hexagonal ice crystals," *J. Atmos. Sci.* **46**, 3–19 (1989).
13. A. Macke, "Scattering of light by polyhedral ice crystals," *Appl. Opt.* **32**, 2780–2788 (1993).
14. J. A. Lock, "Ray scattering by an arbitrarily oriented spheroid. I. Diffraction and specular reflection. II. Transmission and cross-polarization effects," *Appl. Opt.* **35**, 500–531 (1996).
15. K. Muinonen, K. Lumme, J. Peltoniemi, and W. M. Irvine, "Light scattering by randomly oriented crystals," *Appl. Opt.* **28**, 3051–3060 (1989).
16. A. Arking and J. D. Childs, "Retrieval of cloud cover parameters from multispectral satellite images," *J. Clim. Appl. Meteorol.* **24**, 322–333 (1985).
17. M. D. King, Y. J. Kaufman, W. P. Menzel, and D. Tanre, "Remote sensing of cloud, aerosol, and water vapor properties from the Moderate Resolution Imaging Spectrometer (MODIS)," *IEEE Trans. Geosci. Remote Sens.* **30**, 2–26 (1992).
18. W. L. Smith, H. E. Revercomb, R. O. Knuteson, F. A. Best, R. Dedecker, H. B. Howell, and H. M. Woolf, "Cirrus cloud properties derived from high spectral resolution infrared spectrometry during FIRE II. I. The high resolution interferometer sounder (HIS) systems," *J. Atmos. Sci.* **52**, 4238–4245 (1995).
19. J. A. Stratton, *Electromagnetic Theory* (McGraw-Hill, New York, 1941).
20. M. Born and E. Wolf, *Principles of Optics* (Pergamon, Oxford, 1970).
21. J. Zhang and L. Xu, "Light scattering by absorbing hexagonal ice crystals in cirrus clouds," *Appl. Opt.* **34**, 5867–5874 (1995).
22. P. Yang and K. N. Liou, "Light scattering by hexagonal ice crystals: comparison of finite-difference time domain and geometric optics models," *J. Opt. Soc. Am. A* **12**, 162–176 (1995).
23. W. P. Arnott, Y. Y. Dong, and J. Hallett, "Extinction efficiency in the infrared (2–18 μm) of laboratory ice clouds: observations of scattering minima in the Christiansen bands of ice," *Appl. Opt.* **34**, 541–551 (1995).
24. C. F. Bohren and D. R. Huffman, *Absorption and Scattering of Light by Small Particles* (Wiley, New York, 1983).
25. H. C. van de Hulst, *Light Scattering by Small Particles* (Wiley, New York, 1957).
26. P. Yang and K. N. Liou, "Single-scattering properties of complex ice crystals in terrestrial atmosphere," *Contrib. Atmos. Phys.* **71**, 223–248 (1998).
27. W. J. Wiscombe, "Improved Mie scattering algorithms," *Appl. Opt.* **19**, 1505–1509 (1980).
28. K. N. Liou and J. E. Hansen, "Intensity and polarization for single scattering by polydisperse spheres: a comparison of ray optics and Mie theory," *J. Atmos. Sci.* **28**, 995–1004 (1971).
29. A. Macke, M. I. Mishchenko, K. Muinonen, and B. E. Carlson, "Scattering of light by large nonspherical particles: ray-tracing approximation versus T-matrix method," *Opt. Lett.* **20**, 1934–1936 (1995).
30. M. I. Mishchenko and A. Macke, "Incorporation of physical optics effect and computation of the Legendre expansion for ray-tracing phase functions involving δ -function transmission," *J. Geophys. Res.* **103**, 1799–1805 (1998).
31. P. Yang and K. N. Liou, "Light scattering by hexagonal ice crystals: solution by a ray-by-ray integration algorithm," *J. Opt. Soc. Am. A* **14**, 2278–2289 (1997).
32. P. Minnis, K. N. Liou, and Y. Takano, "Inference of cirrus cloud properties using satellite-observed visible and infrared radiances. I. Parameterization of radiance fields," *J. Atmos. Sci.* **50**, 1279–1304 (1993).
33. B. A. Baum, R. F. Arduini, B. A. Wielicki, P. Minnis, and S.-C. Tsay, "Multilevel cloud retrieval using multispectral HIRS and AVHRR data: nighttime oceanic analysis," *J. Geophys. Res.* **99**, 5499–5514 (1994).
34. Q. Han, W. B. Rossow, J. Chou, K.-S. Kuo, and R. M. Welch, "The effect of aspect ratio and surface roughness on satellite retrieval of ice-cloud properties," *J. Quant. Spectrosc. Radiat. Transfer* **63**, 559–583 (1999).
35. M.-D. Chou, K.-T. Lee, S.-C. Tsay, and Q. Fu, "Parameterization for cloud longwave scattering for use in atmosphere models," *J. Climate* **12**, 159–169 (1999).
36. D. L. Mitchell, A. Macke, and Y. Liu, "Modeling cirrus clouds. II. Treatment of radiative properties," *J. Atmos. Sci.* **53**, 2967–2988 (1996).
37. Q. Fu, P. Yang, and W. B. Sun, "An accurate parameterization of the infrared radiative properties of cirrus clouds for climate models," *J. Climate* **11**, 2223–2237 (1998).
38. T. C. Grenfell and S. G. Warren, "Representation of a nonspherical ice particle by a collection of independent spheres for scattering and absorption of radiation," *J. Geophys. Res.* **104**, 31,697–31,709 (1999).
39. D. L. Mitchell, "Parameterization of the Mie extinction and absorption coefficients for water clouds," *J. Atmos. Sci.* **57**, 1311–1326 (2000).
40. A. J. Baran and S. Havemann, "Rapid computation of the optical properties of hexagonal columns using complex angular momentum theory," *J. Quant. Spectrosc. Radiat. Transfer* **63**, 499–519 (1999).
41. S. Warren, "Optical constants of ice from the ultraviolet to the microwave," *Appl. Opt.* **23**, 1206–1225 (1984).
42. Y. Takano and K. N. Liou, "Radiative transfer in cirrus clouds. II. Theory and computation of multiple scattering in an anisotropic medium," *J. Atmos. Sci.* **46**, 20–36 (1989).
43. K.-D. Rockwitz, "Scattering properties of horizontally oriented ice crystal columns in cirrus clouds," *Appl. Opt.* **28**, 4103–4110 (1989).